ADP-Ribosylation Levels and Patterns Correlate with Gene Expression and Clinical Outcomes in Ovarian Cancers

Lesley B. Conrad[1,2,3], Ken Y. Lin[1,2,3], Tulip Nandu[1,2], Bryan A. Gibson[1,2], Jayanthi S. Lea[3], and W. Lee Kraus[1,2]

ABSTRACT

Inhibitors of nuclear PARP enzymes (e.g., PARP-1) have improved clinical outcomes in ovarian cancer, especially in patients with *BRCA1/2* gene mutations or additional homologous recombination (HR) DNA repair pathway deficiencies. These defects serve as biomarkers for response to PARP inhibitors (PARPi). We sought to identify an additional biomarker that could predict responses to both conventional chemotherapy and PARPi in ovarian cancers. We focused on cellular ADP-ribosylation (ADPRylation), which is catalyzed by PARP enzymes and detected by detection reagents we developed previously. We determined molecular phenotypes of 34 high-grade serous ovarian cancers and associated them with clinical outcomes. We used the levels and patterns of ADPRylation and PARP-1 to distribute ovarian cancers into distinct molecular phenotypes, which exhibit dramatically different gene expression profiles. In addition, the levels and patterns of ADPRylation, PARP-1 protein, and gene expression correlated with clinical outcomes in response to platinum-based chemotherapy, with cancers exhibiting the highest levels of ADPRylation having the best outcomes independent of *BRCA1/2* status. Finally, in cell culture-based assays using patient-derived ovarian cancer cell lines, ADPRylation levels correlated with sensitivity to the PARPi, Olaparib, with cell lines exhibiting high levels of ADPRylation having greater sensitivity to Olaparib. Collectively, our study demonstrates that ovarian cancers exhibit a wide range of ADPRylation levels, which correlate with therapeutic responses and clinical outcomes. These results suggest ADPRylation may be a useful biomarker for PARPi sensitivity in ovarian cancers, independent of *BRCA1/2* or homologous recombination deficiency status.

Introduction

Ovarian cancer is the 10th most common cancer among women in the United States (incidence of ∼22,000 cases of ovarian cancer diagnosed per year), but is the 5th leading cause of cancer mortality in women (∼14,000 deaths per year; refs. 1, 2). Ovarian cancer is the most deadly of all gynecologic cancers, with less than 50% of patients surviving 5 years (3). Because early-stage ovarian cancer is difficult to detect, most patients have advanced disease (stage III–IV) at diagnosis (4). Despite advances in radical surgery and chemotherapy for the treatment of advanced ovarian cancers, up to 85% eventually relapse and response to subsequent cytotoxic therapies is short-lived (5).

The first molecular aberrations to be targeted therapeutically in ovarian cancers were germline mutations in genes encoding components of homologous recombination-mediated DNA repair (HRR) pathways (e.g., *BRCA1, BRCA2).* In 2005, two landmark studies demonstrated the effectiveness of PARP inhibitors in *BRCA1/2*-mutated cancers in preclinical models (6, 7). These studies demonstrated efficacy through a mechanism involving synthetic lethality between the PARP inhibitors, which block PARP-mediated DNA repair, and the HRR pathways controlled by BRCA1 and BRCA2 (6, 7). In 2014, the U.S. Federal Drug Administration (FDA) approved the use of the PARP inhibitor Olaparib (Lynparza) as a 4th line agent for recurrent ovarian cancers harboring deleterious germline mutations in *BRCA1* or *BRCA2* (8–10). The FDA has since expanded the use of PARP inhibitors, including Rucaparib (Rubraca) and Niraparib (Zejula), to germline *BRCA1/2*-mutated patients with recurrent epithelial ovarian, fallopian tube, or primary peritoneal cancers after 2 lines of platinum-based chemotherapy (11, 12).

Evidence of potential efficacy of PARP inhibitors in nongermline *BRCA1/2*-mutated ovarian cancers has led to FDA approval of PARP inhibitors for use in certain clinical scenarios regardless of *BRCA1/2* status (13). Given the effectiveness of PARP inhibitors in the HRR pathway, there has been a considerable effort made to develop biomarkers to identify an HRR dysfunction phenotype that could predict PARP inhibitor sensitivity. In addition, given (i) emerging roles of nuclear PARP proteins in molecular pathways beyond DNA repair (e.g., transcription, chromatin regulation, RNA processing; refs. 14, 15) and (ii) potential therapeutic effects of PARP inhibitors in cancers without *BRCA1/2* mutations or observable HRR defects (11, 13, 16), biomarkers for PARP inhibitor responsiveness in these cases are needed as well.

Most of our understanding of the molecular and biological functions of PARPs and the posttranslation modification of proteins that they mediate [i.e., ADP-ribosylation (ADPRylation)] has come from studies with nuclear PARPs, in particular PARP-1, the most abundant

[1]Laboratory of Signaling and Gene Expression, Cecil H. and Ida Green Center for Reproductive Biology Sciences, University of Texas Southwestern Medical Center, Dallas, Texas. [2]Division of Basic Research, Department of Obstetrics and Gynecology, University of Texas Southwestern Medical Center, Dallas, Texas. [3]Division of Gynecologic Oncology, Department of Obstetrics and Gynecology, University of Texas Southwestern Medical Center, Dallas, Texas.

Note: Supplementary data for this article are available at Molecular Cancer Therapeutics Online (http://mct.aacrjournals.org/).

Current address for L.B. Conrad: Division of Gynecologic Oncology, Department of Gynecology and Obstetrics, Emory University, Atlanta, Georgia; current address for Ken Y. Lin, Division of Gynecologic Oncology, Department of Obstetrics and Gynecology, Albert Einstein College of Medicine, New York, New York; and current address for Bryan A. Gibson, Department of Biophysics, University of Texas Southwestern Medical Center, Dallas, Texas.

Corresponding Author: W. Lee Kraus, University of Texas Southwestern Medical Center, Dallas, TX 75390. Phone: 214-648-2388; E-mail: lee.kraus@utsouthwestern.edu

Mol Cancer Ther 2020;19:282–91

doi: 10.1158/1535-7163.MCT-19-0569

and ubiquitous member of the PARP family (14, 15). PARP-1 is a ubiquitously expressed nuclear enzyme that has conserved functional domains for both nonsequence-specific DNA binding and nicotinamide adenine dinucleotide (NAD^+)-dependent catalytic activity (14, 15). Upon activation, PARP-1 uses NAD^+ to catalyze the addition of PAR polymers on itself (i.e., automodification) and other substrate proteins (17, 18). Other PARP family members catalyze the addition of mono(ADP-ribose) (MAR) monomers (14, 18). The levels of protein-linked PAR and MAR are a direct indication of the levels of PARP activity in the cell, as well as the biology of the cell. While few studies have investigated endogenous ADPRylation as a potential biomarker for responses to PARP inhibitor treatment, some progress has been made in this regard, with correlations between the levels of PARylation and responses to PARP inhibitors observed (19, 20).

Currently, the most widely used tool for the detection of PARylated proteins is a monoclonal antibody (10H mAb), which detects polymers of ADP-ribose greater than nearly 10 to 15 units in length (21). The 10H mAb, however, does not detect other products of PARP activity, such as oligo(ADP-ribose) (OAR) and MAR, which are likely to have important biological roles. Our lab has recently developed a set of recombinant antibody-like ADP-ribose detection reagents that can recognize all forms of ADP-ribose, including: (i) pan-ADP-ribose (MAR/OAR/PAR) and (ii) OAR/PAR (22). Various immunological techniques have been developed for detecting PARP-1 proteins and activity levels in cultured cells or clinical tumor samples (23–30). In studies described herein, we used our recombinant antibody-like ADP-ribose detection reagents to characterize the levels and patterns of ADPRylation in a cohort of ovarian cancer tumor tissue samples and relate the results to molecular, cellular, and clinical outcomes. Our results indicate that ADPRylation can be a useful predictive biomarker in ovarian cancers.

Materials and Methods

Tissue and patient data collection

We obtained tissue samples intraoperatively from surgical tumor specimens of patients with high-grade serous ovarian cancer at the time of the planned cytoreductive surgery under a tissue repository protocol from 2009 to 2014. Samples were immediately flash frozen in liquid nitrogen, and stored at −80°C until use. Samples from 34 different patients were used in this study. Patient data were obtained from electronic medical records and included: age, race, stage, histology, laboratory values, debulking status, germline *BRCA* mutation status, chemotherapy regimens, platinum status, and survival outcomes. These studies were conducted in accordance with recognized U.S. and international ethical guidelines, and informed consent was obtained from the patients. This study was performed with approval by the University of Texas Southwestern Medical Center Institutional Review Board (IRB No. #STU-012015-019).

Antibodies

Primary antibodies used for Western blotting were as follows: (i) recombinant antibody-like PAR binding reagent (WWE-Fc; anti-PAR) and pan ADP-ribose binding reagent (Macro-Fc; anti-panADPR), which were expressed in bacteria and purified as previously described (ref. 22; now available from EMD Millipore; catalog nos. MABE1031 and MABE1016, respectively) and (ii) rabbit anti-PARP-1 polyclonal antiserum (generated in the Kraus lab; ref. 31), used at 1:1,000 dilution. Primary antibodies against SNRP70 (Abcam ab83306; 1:4,000 dilution) and TFIID (SI-1; Santa Cruz Biotechnology, sc-273; 1:500 dilution) were used for detection of loading controls. The secondary antibody used for detection was a goat anti-rabbit HRP-conjugated antibody (Thermo Fisher Scientific, 31346; 1:2,500 dilution).

Preparation of nuclear extracts from human ovarian cancers

Frozen tumor samples were homogenized in 1× isotonic lysis buffer (50 mmol/L Tris-HCl pH 7.5, 10 mmol/L $MgCl_2$, 15 mmol/L $CaCl_2$, 1.5 mmol/L sucrose) supplemented with 1 mmol/L dithiothreitol (DTT; Sigma), 1× protease inhibitor cocktail (Sigma), 250 U/μL Universal Nuclease (Thermo Fisher Scientific), 20 μmol/L PJ34 (Sigma), and 500 nmol/L adenosine 5′-diphosphate (hydroxymethyl)pyrrolidinediol (ADP-HPD; Millipore) using a Bullet Blender (Next Advance). The homogenate was subjected to centrifugation for 20 minutes at full speed in a microcentrifuge at 4°C, and the supernatant containing the cytoplasmic extract was collected, flash-frozen, and stored at −80°C for later use. Nuclear extracts were prepared from the pelleted nuclei by adding extraction buffer [20 mmol/L HEPES pH 7.9, 1.5 mmol/L $MgCl_2$, 0.42 mmol/L NaCl, 0.2 mmol/L EDTA, 25% (v/v) Glycerol] supplemented as described above, following a protocol provided with the CelLytic NuCLEAR Extraction Kit (Sigma). The protein concentrations of the nuclear extracts were determined using a Bradford Assay Kit (Thermo Fisher Scientific) and the remaining nuclear extracts were aliquoted, flash-frozen, and stored at −80°C for later use.

Western blotting of nuclear extracts from human ovarian cancers

Ten micrograms of nuclear extract protein from each sample was prepared for SDS-PAGE by adding 4× SDS sample buffer to a final concentration of 1×, followed by incubation for 5 minutes at 100°C. The samples were resolved on 10% PAGE-SDS gels for ADPR and 6% PAGE-SDS gels for PARP-1. The protein gels were transferred to a nylon-backed nitrocellulose membrane. The membranes were blocked for 1 hour at room temperature in tris-buffered saline with 0.1% Tween 20 (TBST) containing 5% nonfat dry milk. Primary antibodies were diluted in 1% nonfat dry milk and incubated for 1 hour at room temperature. After extensive washing in TBST, the membranes were incubated with an HRP-conjugated secondary antibody diluted in 1% nonfat dry milk for 1 hour at room temperature. Signals were revealed using a luminol-based enhanced chemiluminescence substrate (Super-Signal West Pico; Thermo Fisher Scientific) and a ChemiDoc imaging system (Bio-Rad).

Quantification of ADPR signal intensities and PARP-1 protein expression levels

ADPR signal intensities from Western blots performed using the Macro-Fc and WWE-Fc reagents were quantified utilizing ImageJ 1.50*i* software. We standardized the blots based on total protein loaded per lane, which was verified after Western transfer by staining the membrane with amido black. We controlled for background intensity and determined the relative signal intensity for each Western blot lane (single patient or cell line). We normalized between blots and replicates by equalizing the PAR signals from Sample 1, which were consistently among the highest that we obtained with both the Macro-Fc and WWE-Fc reagents. The ratios of the Macro-Fc and WWE-Fc signals were determined by dividing the normalized signals for Macro-Fc by the normalized signals from the WWE-Fc reagent. Similar methods were applied to the PARP-1 signal band of each patient or cell line to determine the relative signal intensity.

Isolation of RNA from human ovarian cancers and polyA+ RNA-seq

Total RNA was isolated from each ovarian cancer tissue sample using an RNeasy Plus Kit (Qiagen), with QIAshredder spin columns for homogenization and on-column DNaseI digestion (79254; Qiagen). The total RNA was analyzed for integrity using an Agilent 2100 Bioanalyzer. The RNA collected was then processed for whole-genome polyadenylated RNA sequencing (polyA+ RNA-seq).

The total RNA samples were enriched for polyA+ RNA using Dynabead Oligo(dT)25 (Invitrogen) and strand-specific RNA-seq libraries were prepared from the polyA+ RNA as described previously (32). The RNA-seq libraries were sequenced using an Illumina HiSeq 2500 (single-end, 50 nt; SE50; one replicate). The RNA-seq data files are available from the NCBI's Gene Expression Omnibus (GEO) portal using accession number GSE136155.

Analysis of RNA-seq data

We used a computational pipeline to analyze the RNA-seq data, which includes the following steps:

(1) RNA-seq read mapping. Single-end RNA-seq reads were aligned to the human reference genome (NCBI 37, hg19) using the spliced read aligner TopHat version 2.0.13 (33) with default parameters.
(2) Transcriptome assembly. The transcriptome for each sample was then assembled using Cufflinks v.2.2.1 (34). We ran Cufflinks using the transcript abundance calculation mode to estimate the read coverage of each transcript.
(3) Differential expression. The assembled transcripts from each individual library were merged using Cuffmerge to generate a master transcriptome. The merged transcripts were then used to determine the FPKM for all transcripts in the patient samples using Cuffdiff.
(4) Filtering transcripts based on a transcript abundance threshold. We obtained transcript abundance, in terms of FPKM, for all transcripts from Cufflinks. A FPKM threshold of 10 was applied to all samples to limit our focus on those transcripts that are reasonably expressed in ovarian cancer tissue samples.

RNA-seq data visualization

Browser tracks

The uniquely mapped reads were converted into bigWig files for visualization in a UCSC genome browser. The writeWiggle function from the groHMM (35) package was used to convert the counts obtained using GRanges to the wiggle file format. The wiggle files were converted to bigwig using wigToBigWig function of the UCSC Genome Browser.

Scatter plots

The FPKM values obtained from the differential expression analysis of the *PARP1* mRNA from RNA-seq were compared with the relative signals from the PARP-1 Western blots (quantified as described above) and used to generate a scatter plot. A similar analysis was performed for the relative signals from the Macro-Fc Western blots versus the relative signals from the PARP-1 Western blots.

Heatmaps

The deviation of expression for each gene in each patient from the mean expression of the gene across all patients was calculated and used to make the heat map. Only those genes with significant deviations were included. The FPKM of the transcripts obtained were subjected to hierarchical clustering using Cluster 3.0 (36) with average linkage to cluster the samples based on the similarity of the expression pattern.

Statistical analyses

Statistical analyses were performed using GraphPad Prism 6. Quantification of Macro-Fc, WWE-Fc, and PARP-1 signal intensities, as well as RNA-seq FPKM, for patients within each of the 4 groups were analyzed using a 1-way ANOVA Tukey–Kramer multiple comparison test. Pearson's correlations were computed to compare Macro-Fc PAR signal intensity to PARP-1 protein expression level, and for PARP-1 protein expression level to *PARP1* mRNA RNA-seq FPKM.

Progression-free survival (PFS) was defined as the time from the date of diagnosis to the date of first recurrence. Overall survival (OS) was defined as the time from the date of diagnosis to the date of death from disease or last follow-up. Kaplan–Meier analyses (37, 38) were used to determine survival outcomes and differences were analyzed with the log rank (Mantel–Cox) test. A P-value < 0.05 was considered significant.

Patient characteristics, including age and pretreatment CA-125 levels (units/mL) were compared using 1-way ANOVA Tukey–Kramer multiple comparison test. The number of patients in each group were compared using a Student t test. Stage at diagnosis (III vs. IV), type of frontline chemotherapy (adjuvant, neoadjuvant, none), surgical residual disease (no gross, optimal, suboptimal), platinum status (sensitive, resistant, refractory), and germline *BRCA* mutation status [negative, *BRCA1* deleterious, *BRCA2* deleterious, *BRCA* variant of unknown significance (*BRCA* VUS), and unknown] were compared using the Chi-square method.

Culture of human ovarian cancer cells lines

OVCAR-3 and OVCAR-4 cells were purchased from the ATCC and were cultured as recommended. HCC5012, HCC5022, HCC5023, HCC5024, HCC5044, and HCC5048 cells were described previously (39) and were obtained directly from the source of the cells (Dr. Adi Gazdar). They were cultured in RPMI1640 medium supplemented with 10% FBS and 2 mmol/L L-glutamine. All cells were used at early passage and were replenished after no more than 15 passages. All cells were verified as mycoplasma-free every 3 months using a PCR-Based Screening Kit.

Preparation of extracts from human ovarian cancer cells lines

Whole cell lysates (WCL) and nuclear extracts were prepared from each ovarian cancer cell line. WCLs were prepared using a high salt extraction buffer [50 mmol/L Tris, pH 7.5, 500 mmol/L NaCl, 1 mmol/L EDTA, 1% NP-40, 10% glycerol, 1 mmol/L β-mercaptoethanol, 1× protease inhibitor cocktail; Roche] containing 10 μmol/L of PJ34 (Sigma) and 500 nmol/L of ADP-HPD (Millipore). After cell lysis, extraction on ice for 30 minutes, and clarification by centrifugation for 20 minutes at full speed in a microcentrifuge at 4°C, the extracts were collected and flash-frozen in liquid N_2. Aliquots were used for determination of protein concentrations using a Bradford assay (Bio-Rad).

Nuclear extracts were prepared using isotonic lysis buffer (10 mmol/L Tris pH 7.5, 2 mmol/L $MgCl_2$, 3 mmol/L $CaCl_2$, and 300 mmol/L sucrose, 1 mmol/L DTT, 1× protease inhibitor cocktail; Roche) containing 10 μmol/L of PJ34 and 500 nmol/L of ADP-HPD. After swelling the cells on ice in isotonic lysis buffer for 15 minutes, cell lysis was induced using 0.6% NP-40. The nuclei were collected by centrifugation on low speed in a microfuge at 4°C and then incubated with extraction buffer (20 mmol/L HEPES, pH 7.9, 1.5 mmol/L $MgCl_2$, 0.42 mmol/L NaCl, 0.2 mmol/L EDTA, 25% glycerol, 1 mmol/L DTT, 1× protease inhibitor cocktail; Roche) containing 10 μmol/L of PJ34

and 500 nmol/L of ADP-HPD at 4°C for 30 minutes with constant shaking. The nuclear extracts were clarified by centrifugation for 20 minutes at full speed in a microcentrifuge at 4°C, collected and flash-frozen in liquid N_2. Aliquots were used for determination of protein concentrations using a Bradford assay (Bio-Rad).

Western blotting of extracts from human ovarian cancer cell lines

For detection of ADPRylation in WCLs and nuclear extracts, 20 μg of lysate from each cell line was used for 8% PAGE-SDS gel electrophoresis. After transfer to a nylon-backed nitrocellulose membrane, the membranes were blotted using the Macro-Fc and WWE-Fc reagents as described above.

Determining cellular sensitivity to Olaparib

The ovarian cancer cell lines noted above were seeded in 96-well polystyrene clear bottom plates (Costar; Catalog No. 3610) and treated with Olaparib for 48 hours, as indicated. Olaparib (MedChem Express, HC-10162) was prepared in DMSO and 1:5 serial dilutions of the drug were prepared. Cell survival was quantified using CellTiter-Glo Luminescent Cell Viability Assay (Promega). Luminescence was measured using Tecan Spark multimode microplate reader (Tecan Trading AG). All experiments were performed with 3 or more biological replicates to ensure reproducibility.

Results

The levels and patterns of ADPRylation and PARP-1 segregate ovarian cancers into distinct molecular phenotypes

Given the importance of PARP-1 in the biology of ovarian cancer and as a therapeutic target (40–42), we hypothesized that the product of PARP activity (i.e., covalent ADPRylation of substrate proteins) might be a good indicator of PARP-1 function in ovarian cancers. We collected tumor tissue from 34 patients with high-grade serous ovarian cancers (the clinical characteristics of the patients and their cancers are presented in **Table 1** and Supplementary Table S1). We used these samples to determine selected molecular phenotypes of the cancers and associate them with patient clinical outcomes (Supplementary Fig. S1).

To determine the relative levels and patterns of protein-linked ADPRylation in these samples, we performed Western blotting of nuclear extracts using 2 recombinant antibody-like ADPR detection reagents previously developed in our lab: (i) Macro-Fc, which detects MAR, OAR, and PAR (pan-ADPR), and (ii) WWE-Fc, which detects, OAR and PAR (ref. 22; **Fig. 1A**). We also monitored PARP-1 protein levels by Western blotting and quantified the signal intensities in arbitrary units for ADPR (from Macro-Fc and WWE-Fc,) and PARP-1 using ImageJ software. We then determined the levels of the Macro-Fc and WWE-Fc signals, as well as their ratios by dividing the normalized signals for each reagent.

To categorize the samples into groups based on the levels and patterns of ADPRylation, we attempted to integrate various parameters from the Western blots, including: (i) WWE-Fc signal, (ii) macro-Fc signal, (iii) macro-Fc/WWE-Fc ratio, (iv) PARP-1 signal, and (v) banding pattern. Initially, we tested a variety of unbiased clustering algorithms using one or more of the quantitative parameters listed above. These analyses yielded a disparate set of results that varied with respect to both the number of clusters and how the samples were distributed within the clusters. Adding some of the clinical parameters from the patients to the clustering analyses did not improve the consistency.

Table 1. Key clinical characteristics of the patients in each ADPRylation group.

	Group			
	1	2	3	4
Number of patients (*n*)	9	15	6	4
Age at diagnosis (years)				
Mean	57	55	50	54
Range	40–77	30–79	45–58	37–63
Stage at diagnosis				
IIIB	1	0	0	1
IIIC	6	9	5	3
IV	2	6	1	0
Mean pretreatment CA-125 (U/mL)	2,832	11,904	1,197	767
Type of chemotherapy				
Adjuvant	9	10	5	4
Neoadjuvant	0	5	0	0
None received	0	0	1	0
Residual disease				
No gross	2	3	1	0
Optimal (≤1 cm)	5	7	3	1
Suboptimal (>1 cm)	2	5	2	3
Platinum status				
Sensitive	9	13	5	2
Resistant	0	0	0	2
Refractory	0	2	1	0
Germline BRCA status				
Negative	2	6	3	2
BRCA1 deleterious	2	3	0	0
BRCA2 deleterious	0	1	1	0
BRCA2 VUS	1	0	0	0
Unknown	4	5	2	2

Thus, we developed a rubric based on cut-offs applied to the WWE-Fc signals and the macro-Fc/WWE-Fc ratio (Supplementary Fig. S2A), which was also guided, in part, by (i) the banding patterns of the ADP-ribose signals, (ii) the PARP-1 signal intensity, and (iii) the most consistent aspects of the unbiased clustering described above (e.g., separation of the samples that comprise groups 1 and 2). This led to the 4 groups of samples shown in **Fig. 1A**. We validated aspects of this approach by using hierarchical clustering with a limited set of the quantitative parameters derived from the Western blots (i.e., WWE-Fc signal, macro-Fc signal, macro-Fc/WWE-Fc ratio). This analysis separated group 1 from the other groups (Supplementary Fig. S2B), as well as group 3 from group 2 at more granular levels of the tree (Supplementary Fig. S2C). Unlike the rubric, this approach did not separate group 4 from group 2 (Supplementary Fig. S2C). For subsequent analyses, we kept the groups 3 and 4 samples distinct from groups 1 and 2, rather than combining them, because of their distinctive patterns, signal intensities, and ratios of macro-Fc/WWE-Fc signals (**Fig. 1A**). Although a number of patient samples had a known deleterious germline mutation in *BRCA1* or *BRCA2* (denoted with an asterisk), these samples were not enriched in any group (**Fig. 1A**; Supplementary Table S1).

We analyzed the quantitative differences in the Western blot signal intensities across the 4 groups using one-way ANOVA Tukey–Kramer multiple comparison tests (**Fig. 1B–E**). The ADPR signals from the Macro-Fc reagent were most intense for Group 1, but did not differ significantly among Groups 2, 3, or 4 ($P < 0.01$; **Fig. 1B**). The ADPR signals from the WWE-Fc reagent showed greater variability among the groups, with the greatest intensity for group 1 ($P < 0.001$; **Fig. 1C**). The ratio of signals from the macro-Fc and WWE-Fc reagents was

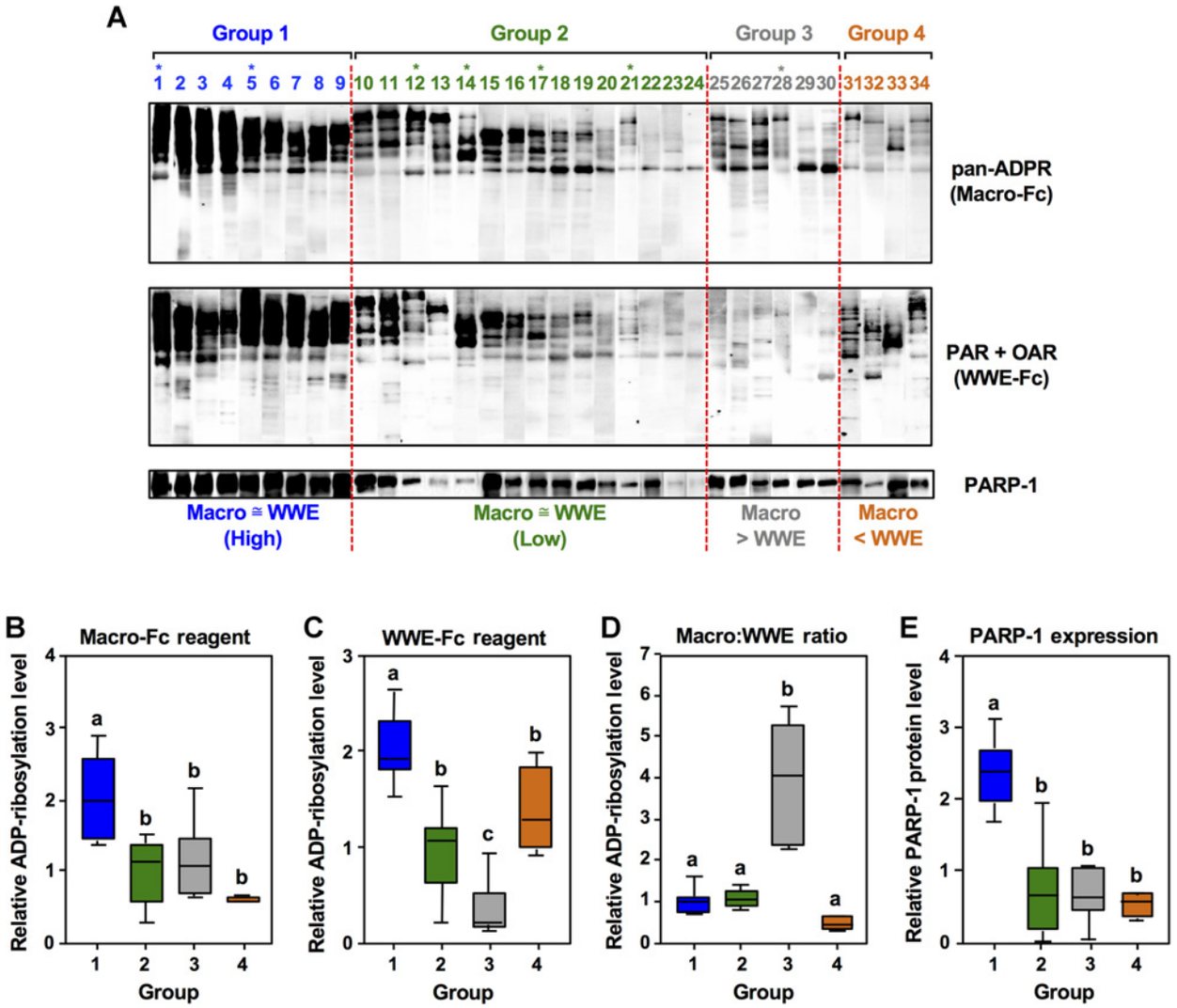

Figure 1.

Determining the relative levels of MAR, OAR, PAR, and PARP-1 in ovarian cancers. **A,** Aliquots of nuclear extract prepared tumor specimens were separated by SDS-PAGE, transferred to nitrocellulose, and subjected to immunoblotting with the macro-Fc and WWE-Fc ADPR detection reagents or PARP-1 antibody, as indicated. Each lane (labeled 1–34) represents a sample collected from a different patient. Differences in ADPR signal intensity yielded 4 ADPRylation groups, each divided by red dashed vertical lines. An asterisk denotes patients who had a known deleterious germline *BRCA1* or *BRCA2* mutation ($n = 7$). Loading was adjusted and standardized so that each lane contained the same amount of total protein. The individual lanes are from control-matched experiments, but have been cut and reordered according to the intensity and pattern of ADPR. **B–E,** Quantification of the Western blot signal intensities for ADPR and PARP-1 in ovarian cancers. **B**, Relative signal from the macro-Fc reagent. **C**, Relative signal from the WWE-Fc reagent. **D**, Ratio of signals for the macro-Fc and WWE-Fc reagents. **E**, Relative PARP-1 protein level. Boxplots representing the ADPR or PARP-1 signal intensity or ratio for each ADPRylation group. The signals were quantified using a ChemiDoc imaging system (Bio-Rad) and expressed in arbitrary units. Each bar represents the mean ± SEM. Group 1 (blue, $n = 9$), Group 2 (green, $n = 15$), Group 3 (gray, $n = 6$), Group 4 (orange, $n = 4$). Bars marked with different letters are significantly different from each other (ANOVA, P-value < 0.05).

significantly different for group 3 ($P < 0.0001$; mean ratio 4.26), as expected, but were not significantly different for group 1 (mean ratio 0.999), group 2 (mean ratio 1.07), and group 3 (mean ratio = 0.46; $P < 0.0001$; **Fig. 1D**). PARP-1 expression levels were significantly greater in group 1 than groups 2, 3, or 4 ($P < 0.0002$), but the expression was not significantly different among groups 2, 3, or 4 ($P > 0.25$; **Fig. 1E**).

Finally, we assessed the potential contribution of PARP-1, the most abundant and active nuclear PARP, to the ADPR signal observed. To do so, we plotted ADPR signal intensity from the macro-Fc reagent versus PARP-1 expression level for all tumor samples ($n = 34$). Using Pearson correlation analysis, we observed a significant positive correlation between ADPR and PARP-1 levels (**Fig. 2A**, Pearson $r = 0.530$, $P = 0.009$). These results suggest that higher levels of ADPRylation are driven by higher PARP-1 protein levels in ovarian cancers. Together, the relative quantification and comparison of ADPR and PARP-1 levels illustrates the molecular differences among the 4 groups.

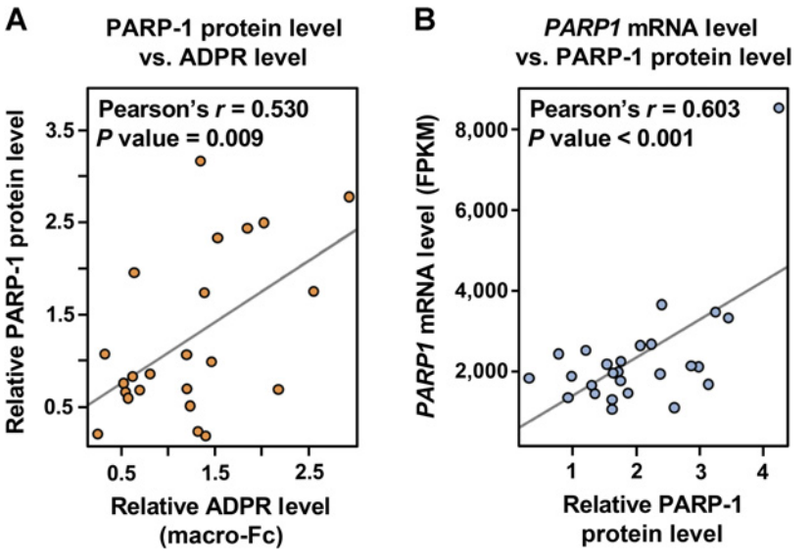

Figure 2.

Correlation of PARP-1 protein levels with ADPR levels and *PARP1* mRNA levels in ovarian cancers. **A,** Pearson's correlation of ADPR levels using the macro-Fc reagent (x-axis) with PARP-1 protein levels (y-axis) from all tumor specimens ($n = 34$). The *P*-value is noted. **B,** Pearson's correlation of PARP-1 protein levels (x-axis) with *PARP1* mRNA levels from RNA-seq (y-axis) from selected tumor specimens ($n = 22$). The RNA-seq is expressed in fragments per kilobase of transcript per Million mapped reads (FPKM). The *P*-value is noted. In panels **A** and **B**, the Pearson's correlation was determined using the ggscatter function in R.

ADPR-defined ovarian cancer groups exhibit dramatically different transcriptomes

To better understand the biological meaning of ADPRylation in ovarian cancers, we sought to relate ADPR levels to gene expression, another frequently used indicator of cancer cell biology. We subjected a subset of patient samples from each group ($n = 22$ total) to RNA sequencing (see Supplementary Table S1 for the samples selected). For our initial analysis using the RNA-seq data, we determined the relationship between *PARP1* mRNA and PARP-1 protein levels. We plotted the mapped reads for *PARP1* mRNA from RNA-seq (fragments per kilobase of transcript per million, FPKM) versus the PARP-1 protein levels from Western blotting (arbitrary units; **Fig. 2B**). Using Pearson correlation, we observed a significant positive correlation between *PARP1* mRNA and PARP-1 protein levels (Pearson $r = 0.603$, $P < 0.001$). Thus, as expected, higher *PARP1* RNA levels correlated positively with higher PARP-1 protein levels.

Next, we assessed the patterns of gene expression across the ovarian cancer samples using the RNA-seq data. We calculated the deviation of expression for each gene in each ovarian cancer sample from the mean expression of the gene across all samples. Only those genes with significant deviations from the average (at least 1 SD) were included, yielding a total of 6,730 significant differentially regulated genes. The FPKM of the transcripts obtained were subjected to hierarchical clustering based on the similarity of the expression patterns. The data were then presented in the heatmap shown in **Fig. 3A**. We also averaged the FPKMs for each gene in the 4 previously derived ADPRylation groups and presented them in the heatmap shown in **Fig. 3B**. Finally, we quantified the expression from the upper (U) and lower (L) one-third of genes represented by the aforementioned heatmap and expressed the results in the boxplots shown in **Fig. 3C**. We observed significant differences across the groups (Wilcoxon rank sum test, *P* value $<2.2 \times 10^{-16}$). Together, these results demonstrate that the gene expression patterns differ dramatically across the 4 ADPRylation groups, suggesting that ADPR levels track with the biology of the cancer types.

We used unbiased clustering of the RNA-seq data to determine if we could observe sample groupings similar to those derived based on the levels and patterns of ADPRylation. We found that k-means clustering separated groups 1 and 2, and to a lesser extent group 3, similar to the rubric and hierarchical clustering used for the Western blot data (Supplementary Fig. S3A). This approach, however, did not separate group 4 from group 2 (Supplementary Fig. S3B), similar to what we observed with the hierarchical clustering used for the Western blot data (Supplementary Fig. S2C). Thus, multiple aspects of our clustering analyses indicate that the ADPRylation and the gene expression results are mutually supportive when it comes to categorizing the samples.

Finally, we defined gene ontologies from the upper (U) one-third and lower (L) one-third of significantly expressed genes (**Fig. 3D**). The genes most highly expressed in group 1 are involved in transcriptional regulation and cellular signaling, whereas the genes most highly expressed in Groups 2 to 4 are involved in cell adhesion, extracellular organization, and inflammatory responses. The gene ontologies for the latter are reminiscent of aggressive cancers, which rearrange their extracellular matrices to alter their ability to adhere and invade surrounding tissues. Collectively, the gene expression analyses described here show that molecular readouts, such as gene expression and ADPRylation levels, can reveal information about cancer cell biology.

The levels and patterns of ADPRylation correlate with clinical outcomes in ovarian cancers

Next, we sought to determine if the levels and patterns of ADPRylation in the 4 groups defined above correlate with clinical outcomes. We plotted Kaplan–Meier recurrence-free (RFS) and overall (OS) survival curves for each of the 4 groups (**Fig. 4A** and **B**). After a median follow-up of 23.5 months, group 1 exhibited significantly better RFS compared with group 4 (median RFS of 22 months vs. 11 months, respectively $P = 0.009$; **Fig. 4A** and **C**). Although the median OS was not reached (NR) for groups 1, 2, and 3; the OS was significantly better for group 1 compared with group 4 (median OS, not reached versus 37 months, respectively, $P = 0.04$; **Fig. 4B** and **C**). Together, these results indicate that the levels and patterns of ADPRylation are indicative of clinical outcomes in ovarian cancers in response to standard-of-care platinum-based therapy.

We note that for group 4, the debulking surgery was optimal in only 25% (1/4) of the patients, compared with 67% (6/9) in group 1, 47% (7/15) in group 2, and 50% (3/6) in group 3 (Supplementary Table S1). Because the status of the debulking surgery is an important prognostic factor in high-grade serous ovarian cancer, we cannot rule out its

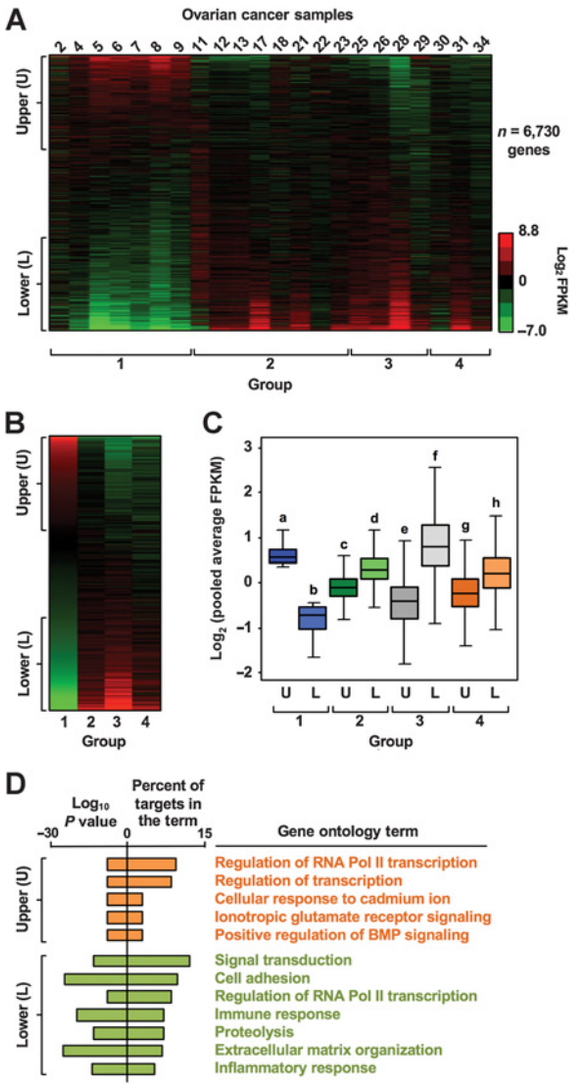

Figure 3.

Different ovarian cancer ADPRylation groups exhibit different gene expression patterns. **A,** Heatmap of RNA-seq data showing the relative expression of 6,730 significantly expressed genes and their associated fold changes in expression calculated from FPKM values for the 22 ovarian cancer samples indicated. The lane numbers correspond to the patient samples in **Fig. 1A**. **B,** Heatmap showing the average FPKM for pooled transcriptomes from each ADPRylation group. The genes were ranked according to a variation filter so as to give higher priority to genes with expression values that have maximum variation across the samples. In this case, we used median absolute deviation (MAD) as the ranking score. The genes that had a MAD less than 10 were excluded from further analysis. A scale bar is shown. **C,** Box plots of the pooled average FPKMs of expressed RNA-seq transcripts for 2 groups of genes defined by the upper (U) and lower (L) expression terciles of group 1 (see **B**). Group 1 (blue), group 2 (green), group 3 (gray), group 4 (orange). Dark colored boxes represent the upper-third and light colored boxes represent the lower-third of expressed transcripts defined by group 1. Bars marked with different letters are significantly different from each other (Wilcoxon rank sum test, P-value $< 2.2 \times 10^{-16}$). **D,** Gene ontologies derived for 2 groups of genes defined by the upper (U) and lower (L) expression terciles of Group 1 (see **B**) using DAVID (version 6.8). The $\log_{10}$ P values and percent of targets in the term are shown for a selection of significant terms.

contribution to the differences seen in RFS with group 4. But, we also we do not have more detailed surgical information to explain additional factors that may have led to suboptimal debulking, which may be complicating covariates.

The levels of ADPRylation correlate with PARP inhibitor sensitivity in patient-derived cell lines

Given the growing importance of PARPi in the treatment of advanced ovarian cancers, as well as the correlations between the levels of ADPRylation and clinical outcomes, as shown in **Fig. 4**, we were interested in determining whether the levels of ADPRylation might also relate to the response of ovarian cancers to PARPi. To explore this possibility, we used 8 patient-derived, high-grade serous ovarian cell lines [HCC lines 5012, 5022, 5023, 5024, 5044, 5048 (39); OVCAR-3, OVCAR-4]. These cells lines exhibited a range of levels of ADPRylation (Supplementary Fig. S4A) and ratios of the signals from macro-Fc and WWE-FC (Supplementary Fig. S4B). Only 2 of the 8 cell lines harbor potential deleterious mutations in *BRCA1/2* (Supplementary Fig. S4A, yellow box). To evaluate PARPi sensitivity, we treated the cell lines with Olaparib, an FDA-approved PARPi, at various concentrations for 48 hours (**Fig. 5A**). We then determined cell survival for all 8 cell lines using a luminescent cell viability assay (Supplementary Fig. S5).

OVCAR-3, which exhibited the highest levels of ADPRylation (**Fig. 5B**; Supplementary Fig. S4A), was the most sensitive to Olaparib (EC_{50} ~1 μmol/L; **Fig. 5C**). In contrast, HCC5048, which exhibited the lowest levels of ADPRylation (**Fig. 5B**; Supplementary Fig. S4A), was largely insensitive to Olaparib (**Fig. 5C**). The relationship was not limited to these 2 cell lines; across the 8 cell lines, sensitivity to Olaparib was strongly and directly correlated with the levels of ADPRylation (in other words, the EC_{50}s for Olaparib were strongly and inversely and correlated with the levels of ADPRylation; Pearson $R = -0.86$, P-value $= 0.0068$; **Fig. 5B** and **D**; Supplementary Figs. S4–S6). As expected, treatment with Olaparib inhibited ADPRylation in the cells (Supplementary Fig. S7).

Based on the levels and patterns of ADPRylation, these 8 cell lines together represented 2 of the patient groups that we defined in **Fig. 1:** groups 1 and 3 (Supplementary Fig. S4A and S4B). The 2 "group 1 similar" cell lines collectively exhibited greater than 50-fold sensitivity to Olaparib compared with the "group 3 similar" cell lines (Supplementary Fig. S8). Whether these group-specific effects hold and are observed for "group 2 similar" and "group 4 similar" cell lines will require further analysis of additional cell lines. Together, our data demonstrate that the levels and patterns of ADPRylation correlate with PARPi sensitivity in patient-derived cell lines. Furthermore, they suggest that ADPRylation levels may be a useful biomarker to predict clinical responses to PARPi.

Discussion

In this study, we sought to identify a new biomarker that could predict responses to both conventional chemotherapy and PARPi in ovarian cancers. We focused on cellular ADPRylation, which we detected using reagents that we developed previously (22). We found that the levels and patterns of ADPRylation and PARP-1 protein segregated 34 high-grade serous ovarian cancers into distinct molecular phenotypes (**Fig. 1**), which exhibit dramatically different gene expression profiles (**Fig. 3**) and clinical outcomes in response to platinum-based chemotherapy (**Fig. 4**). Finally, we found that ADPRylation levels in patient-derived ovarian cancer cell lines correlate with sensitivity to the PARPi Olaparib

Figure 4.

ADPR levels and patterns correlate with clinical outcomes in ovarian cancers. **A** and **B,** Kaplan–Meier survival analyses for each ADPRylation group. **A,** Recurrence-free survival (RFS) and (**B**) overall survival (OS) are shown. **C,** Statistical comparisons from the Kaplan–Meier survival analyses shown in **A** and **B**. Median RFS and OS (in months) were determined for each ADPRylation group (1–4) and the curves were compared using log-rank. Significant comparisons are indicated. Median OS was not reached (NR) for Groups 1 to 3. No other comparisons were significant: RFS: 1 vs. 2 ($P = 0.108$), 1 vs. 3 ($P = 0.137$), 2 vs. 3 ($P = 0.652$), 2 vs. 4 ($P = 0.107$), 3 vs. 4 ($P = 0.119$); OS: 1 vs. 2 ($P = 0.227$), 1 vs. 3 ($P = 0.22$), 2 vs. 3 ($P = 0.949$), 2 vs. 4 ($P = 0.342$), 3 vs. 4 ($P = 0.301$).

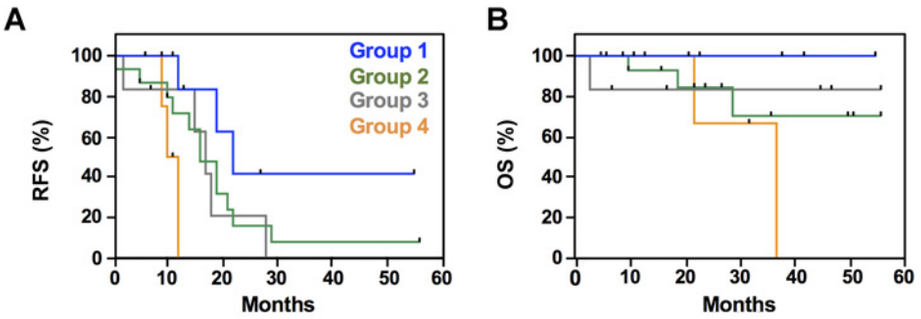

C

ADPR versus clinical outcomes

Clinical outcome	Group 1	Group 2	Group 3	Group 4	Log-rank *P*-value*
Median RFS (months)	22.0	16.0	17.0	11.0	Overall, $P = 0.041$ 1 vs. 4, $P = 0.0091$
Median OS (months)	NR	NR	NR	37.0	Overall, $P = 0.332$ 1 vs. 4, $P = 0.045$

**No other comparisons were significant (see the figure legend).*

independent of *BRCA1/2* status (**Fig. 5**). Collectively, our results suggest that ADPRylation may be a useful biomarker for PARP inhibitor sensitivity in ovarian cancers.

ADPRylation and gene expression in ovarian cancers

The four ADPR-defined ovarian cancer groups exhibited distinct gene expression patterns. In future studies, it may be informative to compare our groupings to similar analyses based solely on gene expression (43). The gene expression analyses revealed cancer-relevant ontologies for the differentially expressed genes, including transcriptional regulation, cellular signaling, cell adhesion, extracellular organization, and inflammatory responses. Some of these gene ontologies are reminiscent of aggressive cancers, which rearrange their extracellular matrices to alter their ability to adhere and invade surrounding tissues (44, 45). Given that the gene expression patterns in a cell are indicative of the biology of the cell or tissue, we can infer that the levels and patterns of ADPRylation are also indicative of the biology of the cell or tissue. Although ADP-ribosylation is likely to be related to therapeutic responses to PARP inhibitors, it may also be more broadly indicative of the biology of the cancer (e.g., aggressive growth). This may make ADP-ribosylation broadly useful as a biomarker in cancers.

Figure 5.

ADPR levels correlate with sensitivity to PARP inhibitor treatment in ovarian cancer–derived cell lines. **A,** Overview of the experimental plan for testing the correlation between PAR levels and sensitivity to PARP inhibitor treatment in 8 different ovarian cancer-derived cell lines. **B,** ADPR and PARP-1 levels in 8 different ovarian cancer-derived cell lines as determined by Western blotting of nuclear extracts using the Macro-Fc reagent and a PARP-1 antibody, respectively. **C,** Assays of cell growth in response to Olaparib treatment for 2 different ovarian cancer cell lines (OVCAR-3 and HCC5048). The surviving fraction relative to the starting number of cells is shown for a wide range of Olaparib concentrations (0.001–100 μmol/L). Each point represents the mean ± SEM, $n \geq 3$. **D,** Pearson's correlation of relative ADPR levels determined using the macro-Fc reagent (from **B**; x-axis) with EC_{50}s for Olaparib sensitivity (from **C** and Supplementary Fig. S5; y-axis) expressed as $\log_2$ of the values. The Pearson r is indicated. The EC_{50}s were determined or extrapolated from the Olaparib sensitivity assays in **C** and Supplementary Fig. S2.

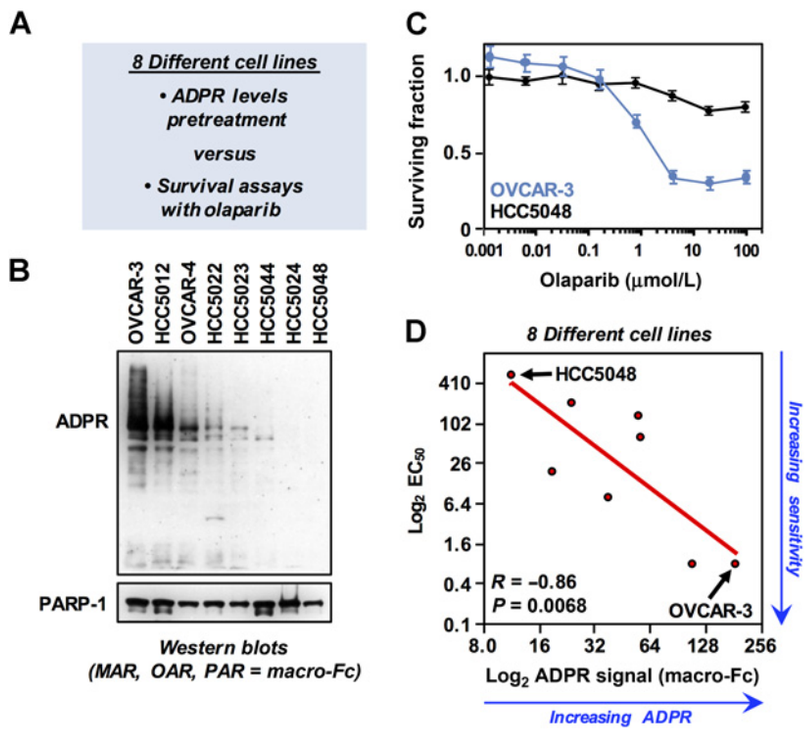

Although one goal of our analyses was to demonstrate that there is biological meaning for protein ADPRylation in a cancer context, we caution that converting this to a meaningful clinical test may be a difficult task. While our study has made headway in this regard, it is not our intention to imply that the groups we defined are necessarily the most clinically relevant way of segregating ovarian cancers. Such conclusions will require a much larger cohort of patient samples. We see our work as pointing the way to what might be possible, rather than an end-all, be-all set of conclusions about clinical states.

Finally, the correlations that we observed between ADPRylation and gene expression outcomes raise the possibility that ADPRylation may play a direct role in gene expression, Although PARP-1 and ADPRylation are known to play key roles in DNA damage surveillance and DNA repair, studies over the past 2 decades have implicated PARP-1 and ADPRylation in the regulation of chromatin structure and gene expression as well (15, 17).

ADPRylation and sensitivity to PARP inhibitors in ovarian cancers

Initial studies of ADPRylation in cancers, mainly PARylation, in cell lines and tumor specimens, have revealed significant variations in ADPRylation levels among different cancer types, as well across individual samples of a given cancer type (19, 20, 30, 46–48). Few studies, however, have investigated endogenous ADPRylation as a potential biomarker for responses to PARP inhibitor treatment. Oplustilova and colleagues observed a correlation between the levels of PARylation and responses to a PARP inhibitor (KU58948; ref. 19). They found that human cancer cell lines with the lowest levels of PAR (i.e., PC3, DU-145) had greater resistance to PARP inhibitor compared with cancer cell lines with higher levels of PAR (i.e., OVCAR 3, U2OS, CAPAN-1).

Similarly, in our studies, we observed the highest sensitivity to the PARP inhibitor Olaparib in patient-derived ovarian cancer cell lines with the highest basal levels of ADPRylation (e.g., OVCAR-3 and HCC5012). These cells resemble the tumor samples found in group 1, which had the highest levels of ADPRylation across all tumor samples. In addition, we observed resistance to Olaparib in patient-derived ovarian cancer cell lines with the lowest basal levels of ADPRylation (e.g., HCC5048 and HCC5024). These cells resemble the tumor samples found in group 3. Interestingly, the Olaparib responses that we observed in the 8 cell lines that we tested were independent of *BRCA1/2* status. Given the gene expression outcomes described above, our results suggest that PARP-1 may be modulating PARP inhibitor sensitivity by activating or repressing specific target genes. Collectively, the results from published studies, as well as our results herein, support the idea that variations in ADPRylation may account for, or at least correlate with, variations in clinical responses to PARP inhibitors.

Our findings of elevated PARP inhibitor sensitivity in ovarian cancer cells with the highest levels of ADPRylation is supported by the work of Gottipati and colleagues (20), who observed hyperactivation of PARP-1 in HRR deficient cell lines and sensitivity to PARP inhibitor in cells with high levels of PAR. We did not observe any obvious relationship between ADPRylation levels and *BRCA1/2* status in our study. However, we did not characterize HRR proficiency in our tumor specimens and cell lines beyond germline *BRCA1/2* mutations. Thus, we cannot exclude the possibility that HRR deficiency is also playing a role in the clinical outcomes that we observed. The relationship between PARP, ADPRylation, and HRR proficiency should be investigated further.

Disclosure of Potential Conflicts of Interest

W.L. Kraus and B.A. Gibson have ownership interest (including patents) in Patent No. 9599606: ADP-ribose detection reagents. W.L. Kraus is a founder and consultant for Ribon Therapeutics, Inc. J.S. Lea is a member of the advisory board for Clovis Oncology. No potential conflicts of interest were disclosed by the other authors.

Dedication

The authors would like to dedicate this paper to A.F. Gazdar, who died in December 2018 during the completion of this work. A.F. Gazdar was a preeminent pathologist and world-renowned lung cancer expert, who shared valuable insights and discoveries of human cancers with the world.

Authors' Contributions

Conception and design: L.B. Conrad, J.S. Lea, W. Lee Kraus
Development of methodology: L.B. Conrad, T. Nandu, J.S. Lea, W. Lee Kraus
Acquisition of data (acquired and managed patients, provided facilities, etc.): L.B. Conrad, K.Y. Lin
Analysis and interpretation of data (e.g., statistical analysis, biostatistics, computational analysis): L.B. Conrad, T. Nandu, W. Lee Kraus
Writing, review, and/or revision of the manuscript: L.B. Conrad, T. Nandu, J.S. Lea, W. Lee Kraus
Administrative, technical, or material support (i.e., reporting or organizing data, constructing databases): L.B. Conrad
Study supervision: J.S. Lea, W. Lee Kraus
Other (prepared reagents used in the manuscript): B.A. Gibson

Acknowledgments

The authors would like to thank Dr. Adi Gazdar, who generated and shared the human ovarian cancer cell lines prior to publication, and advised how best to grow and use them. The authors would also like to thank members of the Kraus lab and the Division of Gynecologic Oncology at UT Southwestern for critical comments and helpful suggestions on this work. This work was supported by a grant from the NIH/NIDDK (R01 DK069710) and funds from the Cecil H. and Ida Green Center for Reproductive Biology Sciences Endowment to W.L. Kraus.

The costs of publication of this article were defrayed in part by the payment of page charges. This article must therefore be hereby marked *advertisement* in accordance with 18 U.S.C. Section 1734 solely to indicate this fact.

Received June 3, 2019; revised August 13, 2019; accepted September 20, 2019; published first October 8, 2019.

References

1. Murphy SL, Xu J, Kochanek KD, Curtin SC, Arias E. Deaths: final data for 2015. Natl Vital Stat Rep 2017;66:1–75.
2. Reid BM, Permuth JB, Sellers TA. Epidemiology of ovarian cancer: a review. Cancer Biol Med 2017;14:9–32.
3. Howlader N, Noone AM, Krapcho M, Miller D, Bishop K, Altekruse SF, et al. SEER Cancer Statistics Review, 1975–2013,National Cancer Institute, Bethesda, MD [cited April 2016]. https://seer.cancer.gov/archive/csr/1975_2013/, based on November 2015 SEER data submission, posted to the SEER web site.
4. Matulonis UA, Sood AK, Fallowfield L, Howitt BE, Sehouli J, Karlan BY. Ovarian cancer. Nat Rev Dis Primers 2016;2:16061.
5. Armstrong DK. Relapsed ovarian cancer: challenges and management strategies for a chronic disease. The Oncologist 2002;7(Suppl 5):20–8.
6. Farmer H, McCabe N, Lord CJ, Tutt AN, Johnson DA, Richardson TB, et al. Targeting the DNA repair defect in BRCA mutant cells as a therapeutic strategy. Nature 2005;434:917–21.
7. Bryant HE, Schultz N, Thomas HD, Parker KM, Flower D, Lopez E, et al. Specific killing of BRCA2-deficient tumours with inhibitors of poly(ADP-ribose) polymerase. Nature 2005;434:913–7.
8. Kaufman B, Shapira-Frommer R, Schmutzler RK, Audeh MW, Friedlander M, Balmana J, et al. Olaparib monotherapy in patients with advanced cancer and a germline BRCA1/2 mutation. J Clin Oncol 2015;33:244–50.

9. Audeh MW, Carmichael J, Penson RT, Friedlander M, Powell B, Bell-McGuinn KM, et al. Oral poly(ADP-ribose) polymerase inhibitor olaparib in patients with BRCA1 or BRCA2 mutations and recurrent ovarian cancer: a proof-of-concept trial. Lancet 2010;376:245–51.
10. Ledermann J, Harter P, Gourley C, Friedlander M, Vergote I, Rustin G, et al. Olaparib maintenance therapy in platinum-sensitive relapsed ovarian cancer. N Engl J Med 2012;366:1382–92.
11. Bitler BG, Watson ZL, Wheeler LJ, Behbakht K. PARP inhibitors: clinical utility and possibilities of overcoming resistance. Gynecol Oncol 2017;147: 695–704.
12. Clamp A, Jayson G. PARP inhibitors in BRCA mutation-associated ovarian cancer. Lancet Oncol 2015;16:10–2.
13. Mirza MR, Monk BJ, Herrstedt J, Oza AM, Mahner S, Redondo A, et al. Niraparib maintenance therapy in platinum-sensitive, recurrent ovarian cancer. N Engl J Med 2016;375:2154–64.
14. Gupte R, Liu Z, Kraus WL. PARPs and ADP-ribosylation: recent advances linking molecular functions to biological outcomes. Genes Dev 2017;31: 101–26.
15. Krishnakumar R, Kraus WL. The PARP side of the nucleus: molecular actions, physiological outcomes, and clinical targets. Mol Cell 2010;39:8–24.
16. Evans T, Matulonis U. PARP inhibitors in ovarian cancer: evidence, experience and clinical potential. Ther Adv Med Oncol 2017;9:253–67.
17. Luo X, Kraus WL. On PAR with PARP: cellular stress signaling through poly (ADP-ribose) and PARP-1. Genes Dev 2012;26:417–32.
18. Gibson BA, Kraus WL. New insights into the molecular and cellular functions of poly(ADP-ribose) and PARPs. Nat Rev Mol Cell Bio 2012;13:411–24.
19. Oplustilova L, Wolanin K, Mistrik M, Korinkova G, Simkova D, Bouchal J, et al. Evaluation of candidate biomarkers to predict cancer cell sensitivity or resistance to PARP-1 inhibitor treatment. Cell Cycle 2012;11:3837–50.
20. Gottipati P, Vischioni B, Schultz N, Solomons J, Bryant HE, Djureinovic T, et al. Poly(ADP-ribose) polymerase is hyperactivated in homologous recombination-defective cells. Cancer Res 2010;70:5389–98.
21. Kawamitsu H, Hoshino H, Okada H, Miwa M, Momoi H, Sugimura T. Monoclonal antibodies to poly(adenosine diphosphate ribose) recognize different structures. Biochemistry 1984;23:3771–7.
22. Gibson BA, Conrad LB, Huang D, Kraus WL. Generation and characterization of recombinant antibody-like ADP-ribose binding proteins. Biochemistry 2017;56: 6305–16.
23. Redon CE, Nakamura AJ, Zhang YW, Ji JJ, Bonner WM, Kinders RJ, et al. Histone gammaH2AX and poly(ADP-ribose) as clinical pharmacodynamic biomarkers. Clin Cancer Res 2010;16:4532–42.
24. Kinders RJ, Hollingshead M, Khin S, Rubinstein L, Tomaszewski JE, Doroshow JH, et al. Preclinical modeling of a phase 0 clinical trial: qualification of a pharmacodynamic assay of poly (ADP-ribose) polymerase in tumor biopsies of mouse xenografts. Clin Cancer Res 2008;14:6877–85.
25. Yang SX, Kummar S, Steinberg SM, Murgo AJ, Gutierrez M, Rubinstein L, et al. Immunohistochemical detection of poly(ADP-ribose) polymerase inhibition by ABT-888 in patients with refractory solid tumors and lymphomas. Cancer Biol Ther 2009;8:2004–9.
26. Kunzmann A, Liu D, Annett K, Malaise M, Thaa B, Hyland P, et al. Flow-cytometric assessment of cellular poly(ADP-ribosyl)ation capacity in peripheral blood lymphocytes. Immun Ageing 2006;3:8.
27. Kummar S, Kinders R, Gutierrez ME, Rubinstein L, Parchment RE, Phillips LR, et al. Phase 0 clinical trial of the poly(ADP-ribose) polymerase inhibitor ABT-888 in patients with advanced malignancies. J Clin Oncol 2009;27: 2705–11.
28. Liu X, Palma J, Kinders R, Shi Y, Donawho C, Ellis PA, et al. An enzyme-linked immunosorbent poly(ADP-ribose) polymerase biomarker assay for clinical trials of PARP inhibitors. Anal Biochem 2008;381:240–7.
29. Fong PC, Boss DS, Yap TA, Tutt A, Wu P, Mergui-Roelvink M, et al. Inhibition of poly(ADP-ribose) polymerase in tumors from BRCA mutation carriers. N Engl J Med 2009;361:123–34.
30. Krukenberg KA, Jiang R, Steen JA, Mitchison TJ. Basal activity of a PARP1-NuA4 complex varies dramatically across cancer cell lines. Cell Rep 2014;8:1808–18.
31. Kim MY, Mauro S, Gevry N, Lis JT, Kraus WL. NAD+-dependent modulation of chromatin structure and transcription by nucleosome binding properties of PARP-1. Cell 2004;119:803–14.
32. Zhong S, Joung JG, Zheng Y, Chen YR, Liu B, Shao Y, et al. High-throughput illumina strand-specific RNA sequencing library preparation. Cold Spring Harb Protoc 2011;2011:940–9.
33. Kim D, Pertea G, Trapnell C, Pimentel H, Kelley R, Salzberg SL. TopHat2: accurate alignment of transcriptomes in the presence of insertions, deletions and gene fusions. Genome Biol 2013;14:R36.
34. Trapnell C, Williams BA, Pertea G, Mortazavi A, Kwan G, van Baren MJ, et al. Transcript assembly and quantification by RNA-Seq reveals unannotated transcripts and isoform switching during cell differentiation. Nat Biotechnol 2010;28: 511–5.
35. Chae M, Danko CG, Kraus WL. groHMM: a computational tool for identifying unannotated and cell type-specific transcription units from global run-on sequencing data. BMC Bioinformatics 2015;16:222.
36. de Hoon MJ, Imoto S, Nolan J, Miyano S. Open source clustering software. Bioinformatics 2004;20:1453–4.
37. Dinse GE, Lagakos SW. Nonparametric estimation of lifetime and disease onset distributions from incomplete observations. Biometrics 1982;38:921–32.
38. Kaplan EL, Meier P. Nonparametric estimation from incomplete observations. J Amer Statist Assn 1958;53:457–81.
39. Thu KL, Papari-Zareei M, Stastny V, Song K, Peyton M, Martinez VD, et al. A comprehensively characterized cell line panel highly representative of clinical ovarian high-grade serous carcinomas. Oncotarget 2017;8:50489–99. doi 10.18632/oncotarget.9929.
40. Franzese E, Centonze S, Diana A, Carlino F, Guerrera LP, Di Napoli M, et al. PARP inhibitors in ovarian cancer. Cancer Treat Rev 2019;73:1–9.
41. Pettitt SJ, Krastev DB, Brandsma I, Drean A, Song F, Aleksandrov R, et al. Genome-wide and high-density CRISPR-Cas9 screens identify point mutations in PARP1 causing PARP inhibitor resistance. Nat Commun 2018;9:1849.
42. Rouleau M, Patel A, Hendzel MJ, Kaufmann SH, Poirier GG. PARP inhibition: PARP1 and beyond. Nat Rev Cancer 2010;10:293–301.
43. Murakami R, Matsumura N, Mandai M, Yoshihara K, Tanabe H, Nakai H, et al. Establishment of a novel histopathological classification of high-grade serous ovarian carcinoma correlated with prognostically distinct gene expression subtypes. Am J Pathol 2016;186:1103–13.
44. Poltavets V, Kochetkova M, Pitson SM, Samuel MS. The role of the extracellular matrix and its molecular and cellular regulators in cancer cell plasticity. Front Oncol 2018;8:431.
45. Walker C, Mojares E, Del Rio Hernandez A. Role of extracellular matrix in development and cancer progression. Int J Mol Sci 2018;19 pii: E3028.
46. Pulliam N, Tang J, Wang W, Fang F, Sood R, O'Hagan HM, et al. Poly-ADP-ribosylation of estrogen receptor-alpha by PARP1 mediates antiestrogen resistance in human breast cancer cells. Cancers (Basel) 2019;11 pii: E43.
47. Kwon M, Jang H, Kim EH, Roh JL. Efficacy of poly (ADP-ribose) polymerase inhibitor olaparib against head and neck cancer cells: predictions of drug sensitivity based on PAR-p53-NF-kappaB interactions. Cell Cycle 2016;15: 3105–14.
48. Herriott A, Tudhope SJ, Junge G, Rodrigues N, Patterson MJ, Woodhouse L, et al. PARP1 expression, activity and ex vivo sensitivity to the PARP inhibitor, talazoparib (BMN 673), in chronic lymphocytic leukaemia. Oncotarget 2015; 6:43978–91.